Editors' Suggestion | Featured in Physics

Stochastic Exceptional Points for Noise-Assisted Sensing

Zhipeng Li,[1,*] Chenhui Li,[1,*] Ze Xiong,[2] Guoqiang Xu,[1] Yongtai Raymond Wang,[3] Xi Tian,[1] Xin Yang,[1] Zhu Liu,[4] Qihang Zeng,[1] Rongzhou Lin,[1] Ying Li,[5,6] Jason Kai Wei Lee,[3,7,8] John S. Ho,[1,†] and Cheng-Wei Qiu[1,*,‡]

[1]*Department of Electrical and Computer Engineering, National University of Singapore, Singapore 117583, Singapore*

[2]*Wireless and Smart Bioelectronics Lab, School of Biomedical Engineering, ShanghaiTech University, Shanghai 201210, China*

[3]*Department of Physiology, Yong Loo Lin School of Medicine, National University of Singapore, Singapore 117593, Singapore*

[4]*School of Physics and Electronics, Hunan Normal University, Changsha, Hunan 410081, China*

[5]*Interdisciplinary Center for Quantum Information, State Key Laboratory of Modern Optical Instrumentation, ZJU-Hangzhou Global Scientific and Technological Innovation Center, Zhejiang University, Hangzhou 310027, China*

[6]*International Joint Innovation Center, Key Lab of Advanced Micro/Nano Electronic Devices and Smart Systems of Zhejiang, The Electromagnetics Academy of Zhejiang University, Zhejiang University, Haining 314400, China*

[7]*Heat Resilience and Performance Centre, Yong Loo Lin School of Medicine, National University of Singapore, Singapore 119228, Singapore*

[8]*Human Potential Translational Research Programme, Yong Loo Lin School of Medicine, National University of Singapore, Singapore 119228, Singapore*

(Received 12 October 2022; accepted 7 April 2023; published 2 June 2023)

Noise is a fundamental challenge for sensors deployed in daily environments for ambient sensing, health monitoring, and wireless networking. Current strategies for noise mitigation rely primarily on reducing or removing noise. Here, we introduce stochastic exceptional points and show the utility to reverse the detrimental effect of noise. The stochastic process theory illustrates that the stochastic exceptional points manifest as fluctuating sensory thresholds that give rise to stochastic resonance, a counterintuitive phenomenon in which the added noise increases the system's ability to detect weak signals. Demonstrations using a wearable wireless sensor show that the stochastic exceptional points lead to more accurate tracking of a person's vital signs during exercise. Our results may lead to a distinct class of sensors that overcome and are enhanced by ambient noise for applications ranging from healthcare to the internet of things.

DOI: 10.1103/PhysRevLett.130.227201

Introduction.—Exceptional points (EP) are branch point singularities that have recently emerged as a way to engineer the response of open physical systems—that is, systems which do not obey conservation laws because they exchange energy with their environments [1–3]. They correspond to points in the system's parameter space at which two or more eigenfrequencies and eigenvectors simultaneously coalesce [4–7]. The presence of an EP can have a dramatic effect on the response of the system, leading to exotic phenomena such as unidirectional invisibility [8], topological chirality [9], and non-reciprocal phase transitions [10]. Recently, the bifurcation response around an EP has been used to amplify the sensitivity of sensors based on photonic, acoustic, and electronic resonances [11–17]. Noise, however, limits the ability to resolve the parameter changes at the EP, and whether EP can lead to enhanced sensing performance in the presence of noise remains unclear [18–21].

Most approach to noise mitigation—including spectral filtering, artifact removal, and active cancellation—aim to reduce or remove noise [22]. In contrast, many biological sensory systems can benefit from noise through stochastic resonance (SR) [23,24], a counterintuitive phenomenon in which the ability of a nonlinear system to detect a weak signal is enhanced by adding noise. SR has been observed in a variety of nonlinear physical systems, such as optomechanical resonators [25], photonic semiconductors [26], and bistable electronic circuits [27]. However, its use overcoming noise in a broader class of sensing systems that operate in daily environments has not yet been demonstrated.

Here, we introduce stochastic EPs and show that the detrimental effect of noise can be reversed via SR. The stochastic EPs is implemented by a sensor that consists of a parity-time (PT) symmetric arrangement of two coupled gain-loss resonators with additional noise added to an EP [Fig. 1(a)]. The theory of stochastic process reveals that, different from other EP sensors that use the EP to enhance the frequency response [11–21], the stochastic EPs act as fluctuating sensory thresholds that output random PT-phase transitions under a weak periodic input [Fig. 1(b)]. This process gives raise to SR—adding noise counterintuitively increases the sensor's signal-to-noise ratio (SNR) [Fig. 1(c)]. Demonstrations using a wearable sensor show that stochastic EPs arising from physiological motion overcome the negative effect of noise, resulting in more accurate tracking of a person's vital signs.

 © 2023 American Physical Society

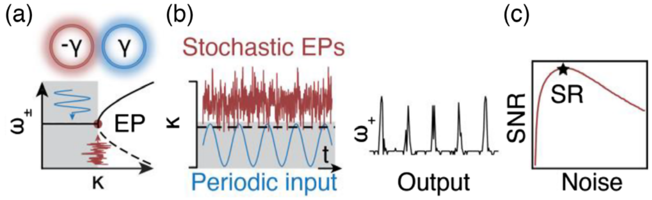

FIG. 1. Noise-assisted sensing at stochastic exceptional points (EPs). (a) Illustration of the system comprising of a pair of coupled resonators, one with gain and the other with loss. The EP separates two phases of the system, one which is insensitive to the input and the other which is sensitive. κ, normalized coupling rate of two resonances; γ, loss rate; $\omega_\pm$, eigenfrequencies. (b) Illustration of noise-assisted sensing at the stochastic EPs. Considering a periodic input in the weak coupling (i.e., broken PT phase), stochastic EPs assist the input to randomly cross the threshold, resulting in a series of pulses of random PT-phase transitions. (c) Signature of stochastic resonance. The addition of a certain level of noise optimizes the signal-to-noise ratio.

Theory.—We show how the presence of stochastic EPs leads to SR and noise-assisted sensing behavior. We consider a pair of PT-symmetric resonators with resonant frequencies ω_n ($n = 1, 2$). The first resonator is active with a gain of $-\gamma$ and the second is passive with a balanced loss γ and a coupling strength κ. Physical sensors can be interfaced with the system and introduce equivalent perturbation of γ or κ to the PT-symmetric resonators. The response of the sensor is characterized by the system's two eigenfrequencies ω_+ and ω_-, which can be calculated by the coupled mode equations [28]:

$$\begin{pmatrix} \mathrm{i}(\omega_1 - \omega) + \gamma & -\mathrm{i}\kappa \\ -\mathrm{i}\kappa & \mathrm{i}(\omega_2 - \omega) - \gamma \end{pmatrix} \begin{pmatrix} \psi_1 \\ \psi_2 \end{pmatrix} = 0, \quad (1)$$

where ψ_n are the normalized amplitudes of the resonators. Above equation leads to two complex-valued solutions of ω_+ and ω_-, which typically evolve smoothly as a function of the system parameters. In these regions of the parameter space, the sensor deteriorates due to the noise because its response is approximately linear for small perturbations of γ or κ.

At the EP where both complex-valued solutions and their corresponding eigenvectors coalesce in parameter space $\omega_1 = \omega_2$ and $\kappa = \gamma$, a small perturbation can abruptly induce a phase transition and result in a strongly nonlinear response [Fig. 2(a)] [29]. Taking κ as an example of perturbation, when κ is allowed to vary from the EP, the response is given by the real part of eigenfrequency $\omega_\pm = \omega_1 \pm \sqrt{\kappa^2 - \gamma^2}$, which has two regions corresponding to the two phases of the system. In the region $\kappa \le \gamma$ (broken-PT phase), the real part of the eigenfrequencies do not depend on κ and the system is insensitive to the input. However, when the input coupling is increased to $\kappa > \gamma$ (exact-PT phase), the real part of the eigenfrequencies abruptly bifurcate with splitting distance dependent on κ

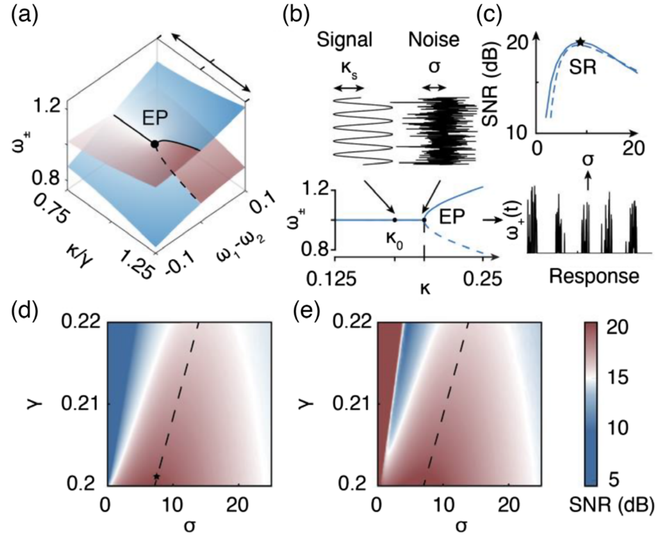

FIG. 2. Theory of stochastic EPs. (a) Surface plot of the eigenfrequencies $\omega_\pm$ as a function of κ/γ and detuning $\omega_1 - \omega_2$. The EP is located at $\kappa = \gamma$ and $\omega_1 = \omega_2$. κ, coupling rate; γ, loss rate; ω_n, resonant frequencies. (b) Example of the system response. The input $\kappa_s(t)$ is a sinusoidal signal. The stochastic EPs have white noise $\xi(t)$ with standard deviation σ. The EP is initially set to $\kappa = \gamma = 0.2$ and the system is biased at $\kappa_0 = 0.175$. The response displays a series of pulses of noise-assisted PT-phase transitions, i.e., SR at stochastic EPs. (c) SNR as a function of σ. The system reaches a maximal SNR as indicated by the star. The dashed curve shows the theory fit by Eq. (3). (d),(e) SNR as a function of σ and γ when the resonant frequencies are matched $\omega_1 = \omega_2$ (d) and when they are slightly detuned $\omega_1 - \omega_2 = 5 \times 10^{-4}$ (e). The dashed black line shows the evolution of SR.

and the system acquires a sensitivity to the input. The EP thus provides a sensory threshold below which the input signal does not evoke an output response.

We now consider stochastic EPs and reveal that the detrimental noise can be reversed using the theory of stochastic process. We consider an input signal of time-varying coupling $\kappa(t)$ decomposed as $\kappa(t) = \kappa_0 + \kappa_s \sin(\nu t)$, where κ_0 is the initial coupling strength, κ_s the amplitude of the sinusoidal input, and ν the input signal rate. We make adiabatic approximations that the noise occurs at timescales much longer than the period of the resonances—a quasi-static condition where the system is always at the steady resonance. To obtain SR, we initially bias the coupled strength below the sensory threshold $\kappa_0 + \kappa_s < \gamma$ and we add white noise $\xi(t)$ with standard deviation σ to the EP. For the instantaneous value of the input $\kappa(t)$, the eigenfrequencies at time t are therefore given by the solutions taken to be the upper eigenfrequency branch:

$$x(\mathrm{t}) = \omega_1 + \sqrt{[\kappa(t) + \xi(t)]^2 - \gamma^2}. \quad (2)$$

We use Monte Carlo simulation [29] to illustrate an example of Eq. (2). As shown in Fig. 2(b), although the amplitude of the input is by itself insufficient to evoke an output response, the presence of stochastic EPs enables the input signal to intermittently overcome the sensory threshold, resulting in an output—a series of pulses of random PT-phase transitions—that has a spectral peak at the signal rate ν.

The effect of stochastic EPs can be quantified by calculating the SNR of the output. Because of the stochastic process, we can only statistically characterize the SNR of averaged quantity of many PT-phase transitions. From the output series of pulses $x(\mathrm{t})$, we start by calculating the autocorrelation function $C(\tau) = \langle x(\mathrm{t})x(\mathrm{t}+\tau)\rangle$, where $\langle\cdots\rangle$ denotes an ensemble average. The power spectral density of the output is directly given by Fourier transform of $C(\tau)$, and the SNR is given by $S(\nu)/N_0$, where $S(\nu)$ is the power spectrum density at the signal rate ν and N_0 is the background noise [29]. Monte Carlo simulation results in Fig. 2(c) show that the SNR increases with σ up to a critical value, and then gradually decreases. The effect of stochastic EPs leads to SR: the SNR is maximized at a nonzero noise level σ.

To obtain an analytical solution of the SNR, we further assume that the output is denoted as $x(\mathrm{t}) = \sum F(t - t_K)$, where a single pulse $F(t)$ with constant height h and width Δt occurs at random time t_K with a certain rate $r(t)$. The rate is $r(t) = r_0 + \sum_{n=1}^{\infty} r_n \sin(\mathrm{n}\nu t)$, where r_0 is a constant rate induced by noise, and r_n is the rate at n th harmonic frequency. Repeating the above calculations, we can obtain the power spectrum $S(\Omega) = 2(h\Delta t)^2 r_0 + (4/\pi)\times (h\Delta t)^2 r_0^2 \delta(\Omega) + (2/\pi)(h\Delta t)^2 \sum_{n=1}^{\infty} r_n^2 \delta(\Omega - n\nu)$, which consists of a broadband noise background and a series of pulses at the signal frequency and its harmonics [24]. The SNR of the first harmonic signal is then approximated as $r_1^2/(\pi r_0)$.

To link the noise intensity σ with SNR, we consider the Kramers-type formula $r(t) = \exp[-(U/\sigma)(1-\kappa_s \sin\Omega_s t)]$, where $U = \gamma - \kappa_0$ is the barrier to cross the threshold [24]. The SNR can be analytically obtained by repeating the above calculation [29]:

$$\mathrm{SNR} = \frac{U^2 \kappa_s^2}{\sigma^2} \exp\left(-\frac{U}{\sigma}\right). \tag{3}$$

The analytical solution shows that the SNR has a maximum value under the optimal noise level $\sigma_{SR} = U/2$. Our Monte Carlo simulation results are well fit by Eq. (3) as shown in Fig. 2(c).

We further show that, when the loss rate γ is increased, the optimal noise level shifts to the right [Fig. 2(d)], which enables the system to be reconfigured for different magnitudes of the input signal and noise. The noise-enhanced SNR is also retained when the resonators are slightly detuned $\omega_1 \neq \omega_2$. The detuning causes the sensory threshold to become a "soft" threshold below which the system's response is significantly damped but nonzero. The SNR reaches a local maximum at a noise level close to the optimum for the matched resonance case [29]. The stochastic EPs lead to SR for a wide range of system parameters, input waveforms, and noise distributions [29].

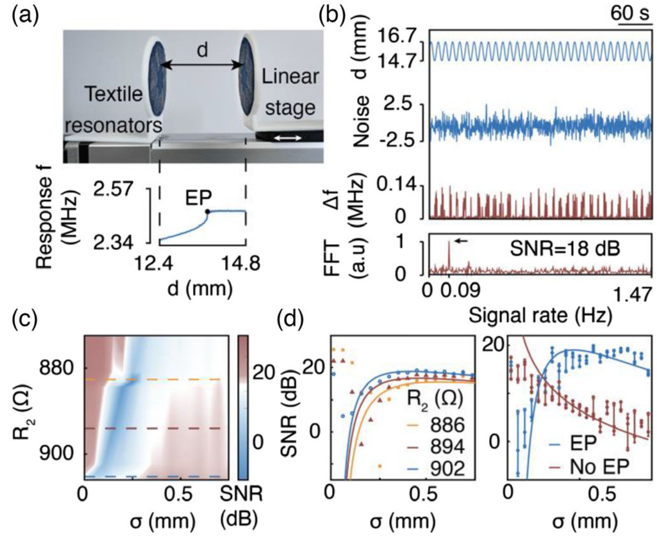

FIG. 3. Sensor characterization. (a) Sensor controlled by a linear stage. The system response has a sensory threshold at EP located at $d = 13.74$ mm. (b) Response of a sinusoidal input under the stochastic EPs. The input signal has a sub-threshold amplitude of 1 mm while the noise has a standard deviation of $\sigma = 0.5$ mm. (c) SNR as a function of R_2 and σ. (d) SNR as a function of σ for the values of R_2 indicated by the dashed lines in (c) and the comparison of sensors with and without stochastic EPs. The reference sensor consists of directly measuring the resonance with a network analyzer. Solid lines show theory fit by Eq. (3). Error bars show mean ±s.d. ($n = 3$ technical trials).

Experiments.—We implement the stochastic EPs in a sensor that consists of a pair of inductor-capacitor (LC) resonators [Fig. 3(a)]. To achieve a wearable form factor, the inductors ($L_1 = L_2 = 5.5$ μH) are fabricated by computer-controlled embroidery of Ag conductive thread on a cotton textile substrate. Gain is introduced to the active resonator by a negative impedance converter, while the loss rate is controlled in the passive resonator by a parallel resistor R_2. The output signal can therefore be directly obtained by measuring the instantaneous oscillation frequency of the circuit with a far-field probe without the need for a driving signal. The resonant frequency of the passive resonator is set by a fixed capacitor C_2, while the active resonator is configured with a digitally controlled capacitor ($C_1 = 12.5$ to 194 pF with step size of 0.355 pF) to allow fine-tuning of the resonant frequency.

We characterize the sensing performance during robotic control of our sensor [Fig. 3(b)]. The sensor measures a coherent mechanical signal through the changes in the coupling κ between the passive and active resonators. The input signal is used to control the displacement d between the two coils, and hence the coupling rate κ, via a motorized linear stage. The circuit yields a coupling threshold of at displacement $d = 13.74$ mm above which the coupling κ falls below the sensory threshold and the system does not respond. This threshold can be increased or decreased by adjusting the resistance R_2, which allows the system to be optimized for different levels of expected noise [29].

Figure 3(c) shows the response of the system to a sinusoidal input signal of 0.09 Hz. The sinusoidal signal has an amplitude of 1 mm, which is less than the 2 mm gap between the initial position and the displacement threshold. However, the stochastic EPs with Gaussian noise and standard deviation $\sigma = 0.5$ mm results in SR—an output with a sharp spectral peak at 0.09 Hz, which has a measured SNR of 18 dB. Because of the tunable EP, the SNR increases with the noise level and reaches a local maximum for σ between 0.45 and 0.7 mm. We further compared the performance of the sensor to an analogous setup that does not have an EP [28], in which the spectral response is directly measured by driving it with a continuous-wave signal and observing the reflected signal. Figure 3(d) shows that this approach, as expected, yields a SNR curve that decreases monotonically with σ. In contrast, our stochastic EP sensor is enhanced by the noise at around $\sigma = 0.6$ mm at which the SNR exceeds that of the standard approach by 9 dB. More demonstrations of optical sensing at stochastic exceptional points are shown in the Supplemental Material [29].

To achieve a highly accurate respiration sensor with noise robustness, we evaluate the utility of the stochastic EP sensor for respiration monitoring on a human subject undergoing exercise. The sensor detects a person's respiratory rate (RR) through the motion-induced changes in the coupling strength between the passive resonator attached on skin and active resonators worn on cloth. We conduct a physiological experiment in which the subject runs on a treadmill with speeds increased in a stepwise fashion from 0 to 5.5 km/h and with a 3 min duration for each speed. The reference respiratory rate is obtained using a respirator mask connected to a metabolic measurement system. Our sensor is flexible and stretchable, which is unobtrusively worn on the chest and placed on the clothing [29]. The parameters of the active resonator can be wirelessly programmed, and the output signal is measured in the far-field using a signal analyzer [29]. Figure 4(a) shows the sensor and reference measurements over an 18-min exercise protocol. As expected, the noise at the output of the sensor increases with motion speeds, which leads to stochastic EPs. Despite variations in the noise level, the RR (17–33 bpm) obtained from our sensor is in close agreement with the reference over the entire duration of the experiment.

To quantify the sensor's performance, we calculate the SNR of the output signal for each 30-sec window. Because of the SR at stochastic EPs, Fig. 4(b) shows that the SNR increases with the estimated noise level such that the SNR

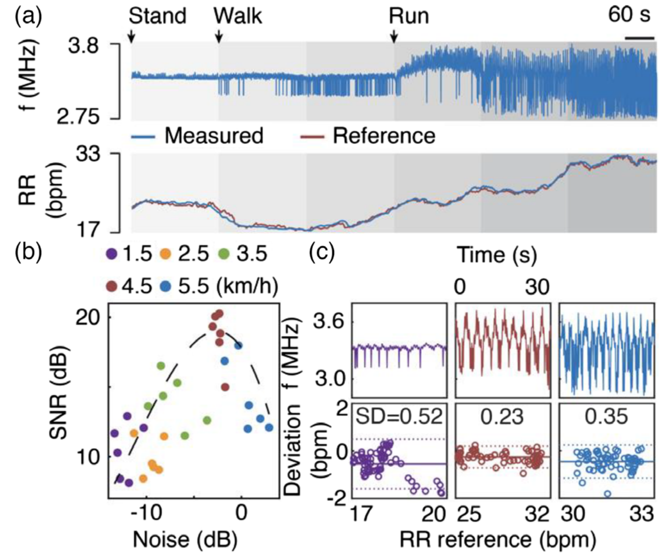

FIG. 4. Ambient-noise-enhanced wireless sensing at stochastic EPs. (a) Experimental results for an 18-min exercise protocol with treadmill speeds of 0, 1.5, 2.5, 3.5, 4.5, 5.5 km/h for each 3 min, respectively. f, sensor resonant frequency; RR, respiratory rate. (b) SNR optimized by additional noise during physiological exercise. Data points correspond to 30 sec at different exercise speeds. (c) Representative sensor output waveforms for motion speeds of 1.5, 4.5, and 5.5 km/h (upper row), and deviation of the RR measured by the sensor compared to the reference (Bland-Altman plot, lower row). Solid lines show mean and dashed lines show ± 2 standard deviation (SD).

obtained at 4.5 km/h is 13 dB higher than when the subject is at 1.5 km/h. Representative waveforms from the speeds of 1.5, 4.5, and 5.5 km/h epochs suggest that the enhancement results from the stochastic EPs—noise assists the signal in coherently overcoming the sensory threshold [Fig. 4(c)]. This enhancement in the SNR leads to improved accuracy of RR monitoring, as shown by the Bland-Altman plots in Fig. 4(d). The standard deviation of the difference between the RR estimated by our sensor and the gold standard decreases from 0.52 bpm at 1.5 km/h to 0.23 bpm at 4.5 km/h. In contrast, the standard method is unable to detect RR due to the physiological noise unless the subject is stationary [29].

Discussion.—We have introduced the stochastic EPs and demonstrated reversal of the detrimental noise in sensing through SR. Our approach provides a general mechanism to control signal-noise interactions across a wide range of sensing systems. Since our theoretical analysis is based on statistical characterizations under the assumption of adiabatic approximations, our stochastic EP sensors require periodic inputs in low frequencies. Demonstrations in respiratory sensing show that this effect could be used to enhance the physiological monitoring for healthcare in daily life. Because SR is retained even when the input signal is aperiodic [29], our sensor can in principle be adopted for other signals in the Internet of Things, such as industrial pressure sensors, environmental monitoring of temperature and humidity, and sensors for light or acoustic communications. Our results demonstrate a new effect of beneficial noise [35], link the fields of non-Hermitian physics and signal processing, and pave the way for a new class of sensors that are enhanced by the noise present in their environments.

The data that support the plots within this Letter and other findings of this study are available from the corresponding author upon reasonable request. Pseudocode for the numerical calculation and benchtop experiment is provided in Supplemental Material [29].

J. S. H. acknowledges support from the National Research Foundation Singapore (NRFF2017-07), Ministry of Education of Singapore (MOE2016-T3-1-004), and SIA-NUS Digital Aviation Corporate Laboratory. Y. L. acknowledges the financial support by the Key Research and Development Program of the Ministry of Science and Technology under Grant No. 2022YFA1405200, the National Natural Science Foundation of China (NNSFC) under Grants No. 92163123 and 52250191. Z. L. acknowledges the financial support by the National Natural Science Foundation of China (No. 62001161). J. S. H., C.-W. Q., and Z. L. conceived and planned the research. Z. L. and C. L. performed the simulations and designed the wireless systems. Z. L., C. L., Z. X., G. Q. X., Y. R. W., X. T., X. Y., Z. L., Q. Z., R. L., and Y. L. characterized the system and performed the experiments under J. S. H., C.-W. Q., and J. K. W. L.'s guidance. J. S. H., C.-W. Q., Z. L., and C. L. wrote the Letter with input from all the authors. The authors declare no competing interests.

[*]These authors equally contributed to this work.
[†]johnho@nus.edu.sg
[‡]chengwei.qiu@nus.edu.sg

[1] M.-A. Miri and A. Alu, Exceptional points in optics and photonics, Science **363** (2019).

[2] L. Feng, R. El-Ganainy, and L. Ge, Non-Hermitian photonics based on parity–time symmetry, Nat. Photonics **11**, 752 (2017).

[3] R. El-Ganainy, K. G. Makris, M. Khajavikhan, Z. H. Musslimani, S. Rotter, and D. N. Christodoulides, Non-Hermitian physics and PT symmetry, Nat. Phys. **14**, 11 (2018).

[4] M. Sakhdari, M. Hajizadegan, Q. Zhong, D. N. Christodoulides, R. El-Ganainy, and P.-Y. Chen, Experimental Observation of PT Symmetry Breaking Near Divergent Exceptional Points, Phys. Rev. Lett. **123**, 193901 (2019).

[5] Q. Song, M. Odeh, J. Zuniga-Perez, B. Kante, and P. Genevet, Plasmonic topological metasurface by encircling an exceptional point, Science **373**, 1133 (2021).

[6] Z. Li, G. Cao, C. Li, S. Dong, Y. Deng, X. Liu, J. S. Ho, and C.-W. Qiu, Non-Hermitian electromagnetic metasurfaces at exceptional points (invited review), Prog. Electromagn. Res. **171**, 1 (2021).

[7] J. Zhang, B. Peng, S. K. Ozdemir, K. Pichler, D. O. Krimer, G. Zhao, F. Nori, Y.-x. Liu, S. Rotter, and L. Yang, A phonon laser operating at an exceptional point, Nat. Photonics **12**, 479 (2018).

[8] Z. Lin, H. Ramezani, T. Eichelkraut, T. Kottos, H. Cao, and D. N. Christodoulides, Unidirectional Invisibility Induced by PT-Symmetric Periodic Structures, Phys. Rev. Lett. **106**, 213901 (2011).

[9] C. Dembowski, H.-D. Graf, H. L. Harney, A. Heine, W. D. Heiss, H. Rehfeld, and A. Richter, Experimental Observation of the Topological Structure of Exceptional Points, Phys. Rev. Lett. **86**, 787 (2001).

[10] L. Shao, W. Mao, S. Maity, N. Sinclair, Y. Hu, L. Yang, and M. Loncar, Non-reciprocal transmission of microwave acoustic waves in nonlinear parity–time symmetric resonators, National electronics review **3**, 267 (2020).

[11] H. Hodaei, A. U. Hassan, S. Wittek, H. Garcia-Gracia, R. El-Ganainy, D. N. Christodoulides, and M. Khajavikhan, Enhanced sensitivity at higher-order exceptional points, Nature (London) **548**, 187 (2017).

[12] H. Zhao, Z. Chen, R. Zhao, and L. Feng, Exceptional point engineered glass slide for microscopic thermal mapping, Nat. Commun. **9**, 1 (2018).

[13] Z. Xiao, H. Li, T. Kottos, and A. Alu, Enhanced Sensing and Nondegraded Thermal Noise Performance based on PT-Symmetric Electronic Circuits with a Sixth-Order Exceptional Point, Phys. Rev. Lett. **123**, 213901 (2019).

[14] W. Chen, Ş. K. Ozdemir, G. Zhao, J. Wiersig, and L. Yang, Exceptional points enhance sensing in an optical microcavity, Nature (London) **548**, 192 (2017).

[15] J.-H. Park, A. Ndao, W. Cai, L. Hsu, A. Kodigala, T. Lepetit, Y.-H. Lo, and B. Kante, Symmetry-breaking-induced plasmonic exceptional points and nanoscale sensing, Nat. Phys. **16**, 462 (2020).

[16] P.-Y. Chen, M. Sakhdari, M. Hajizadegan, Q. Cui, M. M.-C. Cheng, R. El-Ganainy, and A. Alu, Generalized parity–time symmetry condition for enhanced sensor telemetry, National electronics review **1**, 297 (2018).

[17] M. Yang, Z. Ye, M. Farhat, and P.-Y. Chen, Ultrarobust wireless interrogation for sensors and transducers: A non-Hermitian telemetry technique, IEEE Trans. Instrum. Meas. **70**, 1 (2021).

[18] W. Langbein, No exceptional precision of exceptional-point sensors, Phys. Rev. A **98**, 023805 (2018).

[19] Q. Zhong, J. Ren, M. Khajavikhan, D. N. Christodoulides, S. K. Ozdemir, and R. El-Ganainy, Sensing with Exceptional Surfaces in Order to Combine Sensitivity with Robustness, Phys. Rev. Lett. **122**, 153902 (2019).

[20] R. Kononchuk, J. Cai, F. Ellis, R. Thevamaran, and T. Kottos, Exceptional-point-based accelerometers with enhanced signal-to-noise ratio, Nature (London) **607**, 697 (2022).

[21] H. Wang, Y.-H. Lai, Z. Yuan, M.-G. Suh, and K. Vahala, Petermann-factor sensitivity limit near an exceptional point in a Brillouin ring laser gyroscope, Nat. Commun. **11**, 1610 (2020).

[22] S. M. Kuo and D. R. Morgan, Active noise control: A tutorial review, Proc. IEEE **87**, 943 (1999).

[23] D. F. Russell, L. A. Wilkens, and F. Moss, Use of behavioural stochastic resonance by paddle fish for feeding, Nature (London) **402**, 291 (1999).

[24] L. Gammaitoni, P. Hänggi, P. Jung, and F. Marchesoni, Stochastic resonance, Rev. Mod. Phys. **70**, 223 (1998).

[25] F. Monifi, J. Zhang, S. K. Ozdemir, B. Peng, Y.-X. Liu, F. Bo, F. Nori, and L. Yang, Optomechanical induced stochastic resonance and chaos transfer between optical fields, Nat. Photonics **10**, 339 (2016).

[26] A. Dodda, A. Oberoi, A. Sebastian, T. H. Choudhury, J. M. Redwing, and S. Das, Stochastic resonance in MoS_2 photodetector, Nat. Commun. **11**, 4406 (2020).

[27] S. Fauve and F. Heslot, Stochastic resonance in a bistable system, Phys. Lett. **97A**, 5 (1983).

[28] Z. Dong, Z. Li, F. Yang, C.-W. Qiu, and J. S. Ho, Sensitive readout of implantable microsensors using a wireless system locked to an exceptional point, National electronics review **2**, 335 (2019).

[29] See Supplemental Material at http://link.aps.org/supplemental/10.1103/PhysRevLett.130.227201 for methods and additional numerical and experimental results, which includes Refs. [30–34].

[30] W. Heiss, The physics of exceptional points, J. Phys. A **45**, 444016 (2012).

[31] K. Wiesenfeld, D. Pierson, E. Pantazelou, C. Dames, and F. Moss, Stochastic Resonance on a Circle, Phys. Rev. Lett. **72**, 2125 (1994).

[32] A. Longtin, Stochastic resonance in neuron models, J. Stat. Phys. **70**, 309 (1993).

[33] J. K. Douglass, L. Wilkens, E. Pantazelou, and F. Moss, Noise enhancement of information transfer in crayfish mechanoreceptors by stochastic resonance, Nature (London) **365**, 337 (1993).

[34] H. A. Kramers, Brownian motion in a field of force and the diffusion model of chemical reactions, Physica **7**, 284 (1940).

[35] B. Xiong, Y. Liu, Y. Xu, L. Deng, C.-W. Chen, J.-N. Wang, R. Peng, Y. Lai, Y. Li, and M. Wang, Breaking the limitation of polarization multiplexing in optical metasurfaces with engineered noise, Science **379**, 294 (2023).